

1 **Effects of rhamnolipid and carboxymethylcellulose**
2 **coatings on reactivity of palladium-doped nanoscale**
3 **zerovalent iron particles**

4
5
6
7 Sourjya Bhattacharjee¹, Mohan Basnet², Nathalie Tufenkji², Subhasis Ghoshal^{1,*}

8 ¹Department of Civil Engineering, McGill University, Montreal, QC H3A 0C3, Canada

9
10 ²Department of Chemical Engineering, McGill University, Montreal, QC H3A 0C5, Canada

11
12 **Environmental Science and Technology**

13 January 5, 2016

14
15
16
17
18
19
20 *Corresponding author phone: 514-398-6867; fax: 514-398-7361; email: subhasis.ghoshal@mcgill.ca

21

22 **ABSTRACT**

23 Nanoscale zerovalent iron (NZVI) particles are often coated with polymeric surface modifiers for improved
24 colloidal stability and transport during remediation of contaminated aquifers. Doping the NZVI surface with
25 palladium (Pd-NZVI) increases its reactivity to pollutants such as trichloroethylene (TCE). In this study, we
26 investigate the effects of coating Pd-NZVI with two surface modifiers of very different molecular size:
27 rhamnolipid (RL, anionic biosurfactant, M.W. 600 g mol⁻¹) and carboxymethylcellulose (CMC, anionic
28 polyelectrolyte, M.W. 700000 g mol⁻¹) on TCE degradation. RL loadings of 13 to 133 mg TOC/g NZVI
29 inhibited deposition of Pd in a concentration-dependent manner, thus limiting the number of available Pd sites
30 and decreasing the TCE degradation reaction rate constant from 0.191 h⁻¹ to 0.027 h⁻¹. Furthermore, the
31 presence of RL in solution had an additional inhibitory effect on the reactivity of Pd-NZVI by interacting with
32 the exposed Pd deposits after they were formed. In contrast, CMC had no effect on reactivity at loadings up to
33 167 mg TOC/g NZVI. There was a lack of correlation between Pd-NZVI aggregate sizes and TCE reaction
34 rates, and is explained by cryo-transmission electron microscopy images that show open, porous aggregate
35 structures where TCE would be able to easily access Pd sites.

36

37

38 INTRODUCTION

39 Nanoscale zerovalent iron (NZVI) has generated considerable interest for environmental remediation because
40 it can rapidly transform a variety of heavy metal and chlorinated organic contaminants through chemical
41 reduction processes.¹ However, there are challenges associated with efficient utilization of NZVI particles,
42 which include the loss of electrons due to reaction with water² and the passivation of NZVI surface due to
43 formation of oxide layers³, leading to reduced reactivity towards target contaminants. Furthermore, the
44 attractive magnetic forces that exist between NZVI particles lead to significant aggregation and pose a
45 challenge to their transport in contaminated aquifers during *in situ* remediation.⁴⁻⁶ In order to mitigate
46 problems associated with aggregation and stability, NZVI is often coated with surface modifiers such as
47 polyelectrolytes and surfactants to increase the efficiency of their transport in the subsurface.⁶⁻¹²

48 Doping the NZVI surface with palladium (Pd-NZVI) enhances contaminant degradation rates by orders of
49 magnitude compared to bare NZVI particles, and addresses the challenges of the loss of electrons to reactions
50 with water.¹³⁻¹⁷ Typically such rate enhancements are facilitated through the rapid conduction of electrons
51 between the Fe⁰ core and the contaminant via a galvanic couple formation between Fe⁰ and Pd⁰, and/or
52 through the role of Pd⁰ as a hydrogenation catalyst.¹⁸ In the latter process, the rapid degradation of target
53 chlorinated contaminants is facilitated by atomic hydrogen species generated by Pd⁰, from H₂ generated by the
54 reduction of H₂O by Pd-NZVI. A few studies^{7, 8, 14, 19-21} have investigated the reactivity of Pd-NZVI coated
55 with surface modifier polymers or surfactants because *in situ* remediation applications of Pd-NZVI will
56 require colloidal stabilization of the particles, and thus understanding the role of surface modifiers on
57 reactivity is important.

58 A number of different types of surface modifiers have been used in the literature to coat NZVI and Pd-NZVI
59 particles ranging from longer chain polyelectrolytes such as polyvinylpyrrolidone (PVP) and CMC^{8, 14}, to
60 shorter chain surfactants such as rhamnolipid (RL)⁹. He and Zhao¹⁹ synthesized CMC-coated Pd-NZVI with
61 various CMC loadings and observed that the trichloroethene (TCE) degradation rate of the nanoparticles
62 increased with CMC loadings up to an optimum CMC to Fe ratio of 0.0124 and attributed the increase to
63 smaller particle sizes generated by the increasing CMC dose. However, the authors noted that the increase in
64 the degradation rate was not directly proportional to increases in specific surface area. At CMC concentrations
65 higher than the optimum, the TCE degradation rate decreased, and this decrease was attributed to the
66 unavailability of reactive sites caused by adsorption of CMC. Sakulchaicharoen et al.¹⁴ investigated the effects
67 of CMC, PVP (360K and 40K) and guar gum on Pd-NZVI reactivity. The authors reported that some
68 stabilizers such as CMC increased the TCE degradation by an order of magnitude compared to non-stabilized

69 Pd-NZVI while other stabilizers such as PVP 40 K and guar gum reduced the TCE degradation rate. The
70 increase in reactivity was attributed to smaller particle sizes of Pd-NZVI while the decrease in reactivity was
71 attributed to reactive site inaccessibility by TCE. In all of these studies, surface modifiers were pre-grafted to
72 the particle. NZVI particles can be coated with surface modifiers either by post-grafting or pre-grafting¹⁰. For
73 pre-grafting, Fe salt solutions are first mixed with surface modifiers and then chemically reduced to obtain the
74 surface modifier-coated NZVI particle. For post-grafting, surface modifiers are mixed with bare NZVI
75 particles and allowed to adsorb onto the nanoparticle surface. Once the surface modifier-coated NZVI
76 particles are synthesized through either approach, Pd salts are added to the nanoparticles and Pd⁰ deposits are
77 formed on the surface of NZVI yielding the surface modifier coated Pd-NZVI particles. In this study, as well
78 as in other studies^{8, 14, 19, 21}, Pd is added as the last step in the synthesis and after equilibration of NZVI with the
79 surface modifier, to avoid rapid loss of substantial amounts of Fe(0) in reaction with water, before
80 commencement of the TCE reactivity assessment.

81 A few studies provide insights on the impacts of surface modifier on the reactivity of non-palladized NZVI.
82 Phenrat et al.²² reported a decrease in TCE degradation rate constants for NZVI particles post-grafted with 3
83 different polyelectrolytes, namely polystyrene sulfonate, CMC and polyaspartate. The authors cited blockage
84 of surface reactive sites and decrease in availability of aqueous TCE at the NZVI surface due to displacement
85 of the aqueous phase by the adsorbed polymer layers as reasons for decreased reactivity. Sun et al.²³ employed
86 polyvinyl alcohol-co-vinyl acetate-co-itaconic acid (PV3A) in a pre-grafting approach to coat non-palladized
87 NZVI particles and observed that uncoated NZVI and PV3A coated NZVI had similar TCE degradation rates
88 although their mean diameters were 100 and 15 nm, respectively. The authors attributed the similarity in
89 degradation rates of coated and uncoated NZVI particles to equal availability of reactive surface areas.
90 Although PV3A-NZVI were smaller with a higher surface area, it was proposed that a large fraction of its
91 reactive surface was occupied by the adsorbed PV3A molecules and unavailable for direct reaction with TCE.

92 Zhu et al.²⁴ reported that the presence of surfactants (SDS, NPE and CTAB) in solution at low concentrations
93 (below critical micelle concentration) nearly doubled the degradation rate of 1,2,4-TCB by Pd-NZVI. The
94 authors suggested that the surfactants adsorbed to the Pd-NZVI and thereby enhanced the accumulation of the
95 contaminant at the Pd-NZVI surface. The authors noted that at higher concentrations of surfactants in solution,
96 contaminant degradation rates by Pd-NZVI were lower, and speculated that it was likely due to the blocking
97 of the Pd sites.

98 The above studies suggest that the mass of surface modifiers associated with Pd-NZVI or NZVI may influence
99 its reactivity either positively or negatively. Because the Pd deposits are considered as the primary reaction

100 sites on Pd-NZVI particles¹⁸, the influence of the surface modifiers on the Pd deposition and binding of the
101 surface modifiers to the Pd deposits would largely affect the reactivity. However, studies to date have not
102 examined whether the surface modifiers sorb on the NZVI surface (exclusive of the Pd sites) or if sorption to
103 Pd deposits on the surface influence the reactivity. The objective of this study was to assess the effects of
104 sorbed surface modifier concentrations on Pd deposition efficiency and TCE degradation rates for Pd-NZVI
105 particles post-grafted with two different surface modifiers, CMC and RL.

106 CMC (M.W. 700000 g mol⁻¹) is a non-toxic and biodegradable anionic polyelectrolyte and RL (average M.W.
107 600 g mol⁻¹) is an anionic biosurfactant. Further details on the surface modifiers used are provided in Table
108 S1. These surface modifiers have been shown to significantly improve transport (reduce deposition and
109 retention) of Pd-NZVI or NZVI in a variety of groundwater compositions and granular materials in our prior
110 studies.^{9, 10, 25-27} However, there are no reports in literature on how post-grafting Pd-NZVI with CMC or
111 biosurfactants such as RL affects its reactivity. The study also provides information on how surface modifiers
112 of different molecular size interact with Pd nano-deposits. There are very few studies^{9, 28} on colloidal
113 stabilization of NZVI with relatively low molecular weight surface modifiers such as RL, and no studies on
114 effects of reactivity of Pd-NZVI by RL.

115 The effects of surface modifier type and dose on Pd-NZVI reactivity to TCE were evaluated by conducting a
116 series of batch experiments where TCE degradation and end product formation were monitored over time.
117 TCE was chosen as a target contaminant because it is widely used in industry and it is considered to be
118 neurotoxic and carcinogenic^{29, 30}, and has been used as a model contaminant in several studies on NZVI or Pd-
119 NZVI reactivity.^{20, 31, 32} Most studies in the literature have employed the pre-grafting approach in Pd-NZVI
120 reactivity studies.^{14, 19, 33} Because in field applications, the post-grafting method of stabilizing nanoparticles is
121 more easily scalable than the pre-grafting method¹, Pd-NZVI particles were post-grafted with surface
122 modifiers in the reactivity experiments. Surface modifier concentrations were monitored by total organic
123 carbon (TOC) measurements and relationships between sorbed surface modifier concentrations and the extent
124 of palladium deposition on NZVI under different CMC and RL doses were characterized. The surface
125 modifier concentrations were varied up to 167 mg TOC/g NZVI and included concentrations shown to be
126 adequate for significantly enhancing Pd-NZVI transport.^{9, 34-36}

127 **MATERIALS AND METHODS**

128 **Surface modifiers.** Sodium salt of CMC (M.W. 700000 g mol⁻¹) was obtained from Sigma-Aldrich, while
129 rhamnolipid JBR215 (mixture of di-rhamnolipid with M.W. 650 g mol⁻¹ and mono-rhamnolipid with M.W.

130 504 g mol⁻¹) was purchased from Jeneil Biosurfactant Co. (Saukville, WI). Stock solutions of CMC (5 g
131 TOC/L) and RL (10 g TOC /L) were prepared in (DI) water.

132 **Preparation of Pd-NZVI suspensions.** Bare NZVI was obtained as stock slurry from Golder Associates Inc.
133 (Montreal, Canada) who synthesized NZVI by ball-milling of granular iron. The slurry was vacuum-dried and
134 stored under anaerobic conditions. The total iron content was 70% (w/w) as determined by ICP-OES analyses,
135 while the Fe⁰ content was 45% (w/w) as determined by measurement of the mass of H₂ released upon
136 acidification of the NZVI according to methods described elsewhere.³²

137 Surface modifier-coated Pd-NZVI suspensions were prepared in 63 mL vials which were used as batch
138 reactors for the TCE degradation experiments. Bare NZVI particles were suspended in 40 mL N₂-purged DI
139 water and sonicated for 10 min (Misonix sonicator, S-4000) to disperse the aggregated nanoparticles. The
140 sonicated NZVI suspension was then mixed with CMC (13 to 167 mg TOC/g NZVI) or RL (13 to 133 mg
141 TOC/g NZVI) and equilibrated for 20 h by mixing in an end-over-end rotator. The TOC of the supernatant
142 after separation of NZVI particles was analyzed periodically for up to 72 h and no changes were detected after
143 20 h. The NZVI was separated by centrifugation (6500g, 20 min) and then retained in a vial by the use of a
144 super magnet (K&J Magnetics Inc.) while the supernatant containing the unadsorbed surface modifier was
145 decanted. The supernatant was then analyzed with a TOC analyzer.

146 After equilibration, an ethanolic solution of palladium acetate was added to bare or surface modifier-coated
147 NZVI (Pd(O₂CCH₃)₂=1 wt.% of NZVI) and sonicated for 15 minutes in a bath sonicator to achieve deposition
148 of Pd⁰ onto the NZVI particles. The final Pd-NZVI concentration was 150 mg/L. The Pd-NZVI was prepared
149 in an anaerobic glove box (Coy Laboratories, Inc) filled with N₂ (99.9% purity). The freshly synthesized Pd-
150 NZVI was immediately used for TCE degradation studies without removing the excess surface modifier in the
151 solution.

152 **Reactivity studies.** TCE degradation experiments were commenced by adding TCE (>99.5% purity, Sigma-
153 Aldrich) as a methanolic solution to the reaction vials containing 40 mL of surface modifier-coated Pd-NZVI
154 suspension, and 23 mL headspace, to yield a total TCE concentration of 23 mg/L. The vials were sealed with
155 Mininert valve-fitted, Teflon-lined caps.

156 The TCE addition was carried out in the anaerobic glove box. The reactors were then capped and continuously
157 mixed using a table top shaker at 650 rpm at 22 ±1 °C. The reactors were sampled periodically and analyzed
158 for TCE, ethane and ethene. Other reaction products such as acetylene, butenes and dichloroethylenes were
159 not observed in GC-MS analyses (Clarus SQ-8, Perkin Elmer) of headspace samples.

160 **Analytical methods.** The TOC content of surface modifiers was determined using a TOC analyzer (Shimadzu
161 Corp.) and 0.1 g/L TOC corresponds to 0.3 g/L mass concentration of CMC and 0.17 g/L of RL. To account
162 for differences in molecular weights of both the surface modifiers investigated, TOC was used as the basis for
163 comparison of surface modifier doses. TCE was quantified by direct injection of 300 μ L of reactor headspace
164 into a Varian CP 3800 GC with flame ionization detector. Further details on GC operation are provided in the
165 Supporting Information (SI).

166 **Nanoparticle characterization.** X-ray Photoelectron Spectroscopy (XPS) was performed for bare NZVI and
167 surface modifier coated NZVI using a VG Escalab 3MKII instrument to characterize the surface oxide layer.
168 Cryogenic-Transmission Electron Microscopy (Cryo-TEM) was performed on uncoated Pd-NZVI and RL and
169 CMC-coated Pd-NZVI to observe the aggregate structure of nanoparticles in suspension. 3 μ l of sample (Pd-
170 NZVI suspension, 1 g/L) was added to C-Flat 2/2 EM grids (Protochips). Further details on sample
171 preparation and handling are provided in the SI.

172 High Resolution-Transmission Electron Microscopy (HR-TEM) was performed on uncoated Pd-NZVI
173 particles to characterize the size of Pd⁰ on the NZVI, using a Tecnai G2F20 S/TEM, equipped with 4k \times 4k
174 CCD Camera and operated at 200 kV.

175 The hydrodynamic diameters of coated and uncoated Pd-NZVI particles were determined by dynamic light
176 scattering (Zetasizer Nano ZS, Malvern). Size measurements were done at regular intervals of time to assess
177 the extent of aggregation of Pd-NZVI during TCE degradation. Identical mixing conditions and particle
178 concentration (150 mg/L) were used and particle diameters were monitored over time periods equal to the
179 duration as the reactivity studies.

180 The mass of Pd deposited on NZVI particles and free Pd in supernatant was measured using an ICP-OES
181 (Thermo ICap Duo 6500). The surface modifier-coated Pd-NZVI was separated from solution using
182 centrifugation followed by magnetic separation and then the nanoparticles and the supernatant were separately
183 acid digested in aqua regia (3:1 HCl: HNO₃).

184 The mass of surface modifier adsorbed to the NZVI surface (i.e., particles to which Pd had not yet been
185 added) was estimated by measuring the difference between the total surface modifier dose and the surface
186 modifier remaining in the supernatant after equilibration (i.e., 20 h mixing period between NZVI and surface
187 modifier). As mentioned earlier, the NZVI particles were separated from solution using centrifugation and
188 magnetic separation.

189 Fourier transform infrared (FTIR) measurements were carried out on lyophilized RL- and CMC-coated NZVI
190 particles, using a Thermo Nicolet 6500 mid-range instrument equipped with a DTGS detector. Samples were
191 loaded onto a diffuse reflectance cell with a reflective gold booster. All spectra were collected with a
192 resolution of 4 cm^{-1} in the range of $4000\text{-}400\text{ cm}^{-1}$.

193

194 RESULTS AND DISCUSSION

195 **Characterization of Pd-NZVI.** High resolution TEM images of Pd-NZVI particles confirmed the deposition
196 of Pd on NZVI particles (confirmed through EDS shown in Figure S1). Primary sizes of NZVI particles
197 ranged from 25-30 nm while Pd sites were deposited in a random fashion as islets of 3 nm in diameter (Figure
198 1. a1-a2). This is in good agreement with other studies which show Pd deposited as 2-4 nm discrete clusters.^{18,}
199 ^{37, 38}

200

201 XPS analyses revealed the presence of iron oxide and hydroxide species on the surface of bare NZVI and RL-
202 and CMC- coated NZVI. Further details are provided in the SI.

203 **Effect of surface modifier loading on TCE degradation rate.** The amount of CMC or RL used to coat the
204 Pd-NZVI particles was varied up to 167 mg TOC/g NZVI, in order to study the effect of surface modifier
205 loadings on TCE degradation rates. The reaction vials had stoichiometrically excess Pd-NZVI relative to TCE.

206 Each data point in Figure 2 represents the pseudo first-order TCE degradation rate constant (k_{obs}) obtained
207 from TCE degradation profiles (Figures S3 and S4) from triplicate reactors for each total surface modifier
208 loading used. For RL loadings from 33 to 133 mg TOC/g NZVI, only the first three data points from time 0
209 were used to calculate the k_{obs} (Figure S3), as no further degradation was observed thereafter. The reason for
210 this inhibition of reactivity is discussed in the following section. For all other cases of coated and uncoated
211 Pd-NZVI, all the experimental data points were fitted to the pseudo first-order rate law ($r^2 > 0.98$) to determine
212 k_{obs} . The k_{obs} values were corrected for partitioning of contaminant between aqueous and gaseous phases, using
213 methods described elsewhere³⁹ and in the SI.

214 As observed in Figure 2, depending on their loading, the Pd-NZVI coated with the two surface modifiers show
215 distinctively different effects on TCE degradation rates. Uncoated bare Pd-NZVI particles yielded a k_{obs} of
216 $0.191(\pm 0.001)\text{ h}^{-1}$, and coating the nanoparticles with varying concentrations of CMC did not have any
217 significant effect on the TCE degradation rate constant (one-way ANOVA, $p > 0.05$). In contrast, increasing the
218 RL loading in the reaction vials containing Pd-NZVI caused a progressively significant decrease in the k_{obs} . At

219 133 mg TOC RL/g NZVI, the TCE degradation rate was only $0.027(\pm 0.001) \text{ h}^{-1}$. Losses due to leakage from
220 vial or sample handling were negligible and >90% mass balance of carbon was obtained for all systems
221 (Figure S5). All experiments were carried out below the critical micellar concentration of RL (30 mg TOC/L⁹)
222 and no partitioning of TCE to only RL or only CMC solutions were measured.

223 An important observation was made by Phenrat et al.²² in the context of non-palladized NZVI post-grafted
224 with polyelectrolytes. The authors observed that the rate of TCE degradation decreased when polyelectrolytes
225 were adsorbed to the NZVI surface and attributed it to the blocking of surface reactive sites at low
226 concentrations of adsorbed polyelectrolytes (between 0.3 to 1.6 mg/m² surface excess, for different
227 polyelectrolytes), and a combination of site blocking and reduced availability of aqueous TCE at the NZVI
228 surface at higher surface excess concentrations. The role of site blocking with respect to Pd-NZVI in our study
229 is discussed in a later section. However, the reduced availability of aqueous TCE at the Pd sites is unlikely
230 because Pd nano-islets could only be deposited at sites which are not blocked by the adsorbed surface modifier
231 coatings.

232 To investigate the differences in reactivity rates observed between bare Pd-NZVI and surface modified Pd-
233 NZVI, three possible ways in which surface modifiers could potentially alter the reactivity of Pd-NZVI were
234 investigated: (a) changes caused in aggregate sizes, (b) changes in Pd deposition on the NZVI particles in the
235 presence of surface modifiers, and (c) interaction of surface modifier molecules in solution with the Pd-NZVI.

236 In previous studies, aggregation of NZVI particles has often been associated with a loss in contaminant
237 degradation rates by NZVI, in that a loss of nanoparticle surface area due to aggregation results in a decrease
238 in sites available for contaminant degradation.^{7, 40, 41} By stabilizing Pd-NZVI with surface modifiers, one
239 would expect improved reactivity of Pd-NZVI due to the significantly smaller aggregate sizes and higher
240 surface area than uncoated Pd-NZVI. The nanoparticle sizes were determined for uncoated Pd-NZVI, and
241 coated Pd-NZVI at two different representative loadings for each type of surface modifier, at 13 mg TOC/g
242 NZVI and 67 mg TOC/g NZVI, in order to probe whether surface modifier loading influenced the extent of
243 Pd-NZVI stabilization which then caused the differences in the TCE degradation rate constants observed in
244 Figure 2. Average diameters of uncoated Pd-NZVI particles were approximately 1500 nm whereas Pd-NZVI
245 coated with both RL and CMC at the selected total surface modifier loadings were 300 nm (Table S2). Despite
246 such significant differences in sizes between uncoated and coated Pd-NZVI, CMC-coatings did not improve
247 Pd-NZVI reactivity while RL-coatings had an adverse effect on reactivity.

248 Because aggregate sizes did not correlate with changing degradation rates, the effect of sorption of surface
249 modifiers to the NZVI surface on Pd deposition was probed along with the interaction of excess surface

250 modifier molecules with the Pd-NZVI. The lack of correlation between particle size and Pd-NZVI reactivity is
251 also explored in a later section.

252 **Palladium deposition studies.** To investigate whether the presence of surface modifier adsorbed on the
253 surface of NZVI can cause changes in Pd deposition, Pd mass loadings (% w/w NZVI) on NZVI surface were
254 characterized at three different total surface modifier loadings: 13, 33 and 67 mg TOC/g NZVI. Figure 3
255 demonstrates the difference in the deposition of Pd on the NZVI particles by the two surface modifiers. The
256 nominal dose of Pd on NZVI particles was 0.5% w/w of NZVI across all reactors with the different CMC and
257 RL doses. However, as shown in Figure 3, Pd deposits on the NZVI to different extents when CMC and RL
258 are used as surface modifiers. CMC has little effect on the deposition of 0.5% Pd (w/w NZVI) on the NZVI
259 surface. In contrast, Pd deposited onto NZVI decreased with an increase in RL loading. The concentration of
260 deposited Pd was 0.35(\pm 0.01)% at 13 mg TOC/g NZVI which decreased to 0.13(\pm 0.02)% at 67 mg TOC/g
261 NZVI. For RL coated Pd-NZVI, a decrease in Pd deposition between 13 and 67 mg TOC/g NZVI
262 corresponded to a decrease in TCE degradation rate constants from 0.145 h⁻¹ to 0.045 h⁻¹, whereas for Pd-
263 NZVI coated with CMC up to 167 mg TOC/g NZVI, no effect on TCE degradation or Pd deposition was
264 observed, suggesting that changes in Pd deposition affects the reactivity of the coated Pd-NZVI particles.
265 However it should be noted that at total RL loadings of 33 and 67 mg TOC/g NZVI, reactivity of Pd-NZVI is
266 also affected by the presence of RL in solution in addition to changes in Pd loading, as discussed in the next
267 section.

268 The differences in Pd deposition on RL-coated NZVI and CMC-coated NZVI may be attributable to
269 differences in sorption of the two surface modifiers and the configuration of the surface modifier molecules on
270 the NZVI surface, both of which could affect the number of reactive sites and surface area available for Pd
271 deposition. Thus, the adsorption of the two surface modifiers on NZVI during the post-grafting process was
272 verified using adsorption isotherm experiments. Figure 4a presents the amount of surface modifier adsorbed
273 onto the NZVI particles at equilibrium as a function of total surface modifier loading. There is a significant
274 difference in the affinity of the two coatings to the NZVI surface with the adsorption of RL being considerably
275 higher than CMC. For instance, approximately 12 mg TOC of CMC/g NZVI was adsorbed at a total CMC
276 loading of 67 mg TOC/g NZVI, whereas, 48 mg TOC of RL/g NZVI was adsorbed to NZVI at an identical
277 total RL loading. Furthermore, it should be noted that CMC in solution exists at all surface modifier loadings
278 investigated, while RL in solution was measured only at and above 33 mg TOC/g NZVI. To characterize the
279 nature of bonding of CMC and RL onto NZVI surface, FTIR measurements were carried out on surface-
280 modified NZVI particles coated with CMC or RL. Both CMC and RL were found to interact with the NZVI
281 through the carboxylate group (Figures S6 and S7).

282 All RL was completely sorbed to NZVI surface for total RL doses up to 20 mg TOC/g NZVI, while the
283 adsorption of RL to NZVI surface from loadings between 33-133 mg TOC/g NZVI could be described using
284 the Langmuir isotherm as shown in Figure 4b. The adsorption of CMC to NZVI surface, at the surface
285 modifier loadings employed, was best described using the Freundlich isotherm as shown in Figure 4c. It
286 should be noted here that Phenrat et al.¹¹ found that 700K CMC sorption to NZVI was best described by a
287 Langmuir isotherm. The difference in the adsorption behaviour of CMC to NZVI compared to our study may
288 be due to differences in the solution chemistry (pH of 7.2 in our study versus pH range of 9.5 to 10.5 in theirs)
289 and NZVI surface chemistry related to differences in particle synthesis methods. Nevertheless, NZVI particles
290 in our study as well as by Phenrat et al. were negatively charged at the pH employed. CMC sorbs significantly
291 less compared to RL and has a different sorption behavior as shown in Figure 4a and discussed above, likely
292 due to differences in molecular size and structure (Table S1). Although CMC sorbed on NZVI, we observed
293 no decrease in k_{obs} for CMC coated Pd-NZVI. This is likely due to limited blocking of Pd deposition sites on
294 the NZVI due to a more open configuration (increased amounts of loops and tails) of the polyelectrolyte due
295 to its macromolecular structure at higher concentrations.^{8, 22} In contrast, the significantly smaller RL molecules
296 likely adsorb in a flat conformation and form a more compact coating on the NZVI surface.^{24, 42}

297 RL has been previously reported to complex with a number of different metal ions⁴³. Thus, we investigated the
298 extent to which free RL in solution (present at total RL loadings of 33 to 133 mg TOC RL/g NZVI)
299 complexed Pd²⁺. In a separate experiment, we contacted uncoated NZVI and a suspension of RL-Pd²⁺ for 15
300 minutes (a time period which was insufficient for RL sorption to NZVI as determined by TOC analyses, but
301 sufficient for Pd reduction and deposition on NZVI). The NZVI was then separated and analyzed by ICP-OES
302 to quantify the amounts of Pd associated with the particles. Because no RL sorbed, the Pd associated with
303 NZVI can be attributed to Pd⁰ derived from the non-complexed Pd²⁺ in the RL-Pd²⁺ suspension. The amount
304 of Pd⁰ that did not deposit on NZVI was assumed to be complexed with RL. The experimental procedures are
305 further explained in the SI and in Figure S8. Using the knowledge of the amounts of Pd complexed by RL in
306 solution, we calculated that in a representative system having a total RL loading of 67 mg TOC RL/g NZVI,
307 for a nominal dose of 0.03 mg Pd (0.5% w/w NZVI), (i) 0.009 mg Pd (0.15% w/w NZVI) was complexed by
308 the 3 mg TOC/L RL in solution, while (ii) 0.0078 mg Pd (0.13% w/w NZVI) was deposited as Pd⁰ on the
309 NZVI surface coated with 48 mg TOC/g NZVI of RL, and (iii) 0.0132 mg Pd (0.22% w/w NZVI) remained in
310 solution (not deposited) and as non-complexed Pd²⁺. This suggests that surface sorbed RL plays a more
311 significant role in controlling the overall Pd⁰ deposition because a large fraction of non-complexed Pd²⁺ was
312 unable to deposit on NZVI. The calculation are further explained in the SI.

313

314 Figure 5 presents a schematic showing these processes including the role of excess surface modifier in
315 solution on TCE degradation, which is discussed below.

316 **Effect of excess surface modifiers in solution on TCE degradation rate.** For all CMC loadings and RL
317 loadings of 13 and 20 mg TOC/g NZVI, all of the TCE in the vials was degraded in less than 40 h. However,
318 at RL loadings of 33 to 133 mg TOC RL/g NZVI, less than 20% of the TCE was degraded over 7 h and
319 thereafter there was no further degradation (Figure S3).

320
321 We investigated whether the incomplete degradation was associated with the presence of excess RL in
322 solution at total loadings ranging from 33 to 133 mg TOC RL/g NZVI (Figure 4). We hypothesized that some
323 of the RL in solution was able to coat the Pd⁰-nanodeposits after their formation and make the Pd⁰ unavailable
324 for TCE dechlorination. This hypothesis was verified by (a) studying the sorption kinetics of RL to Pd⁰
325 surfaces (created by synthesizing Pd⁰ nanoparticles) and (b) conducting TCE degradation experiments with
326 and without excess RL present in solution. The sorption of RL to Pd⁰ fitted a Langmuir isotherm (Figure S9),
327 thus suggesting that coating of Pd⁰ deposits by RL from the solution phase can occur after formation of the
328 Pd⁰ nanodeposits. To investigate the consequences of RL sorption to Pd⁰ on the reactivity of Pd-NZVI, two
329 identical sets of reactors were prepared in which NZVI particles were first coated with 67 mg TOC of RL/g
330 NZVI. After the NZVI particles had equilibrated with RL, Pd nano-deposits were formed by adding Pd-
331 acetate. Then, one set of triplicate reactors was maintained as is (i.e. with excess RL in solution), while in the
332 other set of triplicate reactors, the excess RL in solution was removed immediately after Pd⁰ deposition by
333 decanting the supernatant (after centrifugation and retention of the Pd-NZVI particles using a supermagnet).
334 The particles in the reactor set without RL in solution, were resuspended in fresh deionized water and
335 subsequently tested for TCE degradation. It was confirmed with TOC analysis that RL did not desorb from the
336 nanoparticles after the resuspension step. A schematic of the reactor sets tested for TCE degradation is shown
337 in Figure 6b and 6c.

338
339 As shown in Figure 6a, the system without any RL in solution, was able to degrade TCE in the reactor
340 completely, while the system with excess RL in solution was able to achieve only 20% reduction.

341
342 Therefore, changes in TCE degradation rates observed for Pd-NZVI coated with RL is caused by two
343 processes: (a) reduction in Pd deposition caused due to sorption of RL to NZVI surface, and (b) coating of
344 deposited Pd⁰ by the excess RL from the solution phase. The amounts of deposited Pd have been discussed
345 earlier and are shown in Figure 3. Depending on the total loading of RL, either one or both processes may be

346 involved in altering the reactivity of Pd-NZVI. Conversely, CMC adsorbed to NZVI surface or present in
347 solution do not affect the reaction rates of Pd-NZVI particles. A schematic outlining the effects of the two
348 surface modifiers on Pd-NZVI is presented in Figure 5.

349 **Aggregation and reactivity.** The lack of relationship between aggregate sizes and Pd-NZVI reactivity was
350 further probed by carrying out Cryo-TEM analysis on suspension droplets of uncoated and coated Pd-NZVI
351 particles, in order to observe their aggregate morphology *in solution*. Cryo-TEM avoids the artefacts
352 associated with drying of the sample which may result in aggregation of nanoparticles during sample
353 preparation for regular TEM imaging. Images show that uncoated Pd-NZVI formed large (~900 nm), open,
354 porous aggregate structures in solution whereas RL- or CMC-coated Pd-NZVI formed smaller (~200 nm)
355 aggregates of fewer nanoparticles (Figure 1. b1-b3). Given the open and porous morphology of the Pd-NZVI
356 aggregates, the degradation rate of TCE by Pd-NZVI is more likely to be dependent on the mass loading of
357 Pd on NZVI rather than aggregate size, because access of TCE to the Pd sites (where TCE degradation
358 primarily takes place¹⁸) is unlikely to be hindered with increase in aggregate size.

359 He and Zhao¹⁹ reported that changes in CMC-coated Pd-NZVI particle sizes from 200 to 18.6 nm (11 times
360 increase in surface area) did not proportionately enhance reactivity rates (1.7 times increase). Additionally, our
361 analysis of their graphical data reveals that there was no statistical difference (one-way ANOVA, $p > 0.05$) in
362 the TCE degradation rate constants for CMC-coated Pd-NZVI with CMC:Fe molar ratios of 0.0093 to 0.0186.
363 The authors observed a statistically significant decrease in rate constants only at a high CMC:Fe ratio of
364 0.061, a dose much higher than those used in our study. Sakulchaicharoen et al.¹⁴ also reported only a 1.3 fold
365 increase in TCE degradation rate constant for CMC-coated Pd-NZVI sizes between 18.8 nm and 2.4 nm (7.7
366 times increase in specific surface area). It should be noted that He and Zhao¹⁹ observed a 8 fold lower
367 reactivity rate of uncoated Pd-NZVI compared to CMC-coated Pd-NZVI. That difference in reactivity is likely
368 due to the different morphology and composition of the uncoated NZVI, which had a dendritic, floc-like
369 morphology, compared to the CMC-coated particles which existed as solid, spherical particles.^{7, 8} However,
370 because the authors did not measure the Pd mass deposition, it is difficult to ascertain the exact reasons for
371 differences in reactivity. In this study, the uncoated and coated non-palladized NZVI had an identical
372 composition as CMC was post-grafted, and thus the only changes that occurred upon CMC-coating was the
373 change in aggregation state as shown in Figure 1 (b1-b3), which did not alter the reactivity of the particles to
374 TCE.

375

376 **IMPLICATIONS**

377 A number of different studies in the literature have focused on reducing Pd-NZVI aggregate size to enhance
378 mobility in the subsurface as well as improve their reactivity to target contaminants. We have demonstrated
379 through this study, that aggregate morphology rather than size plays an important role in determining Pd-
380 NZVI reactivity. A significant factor determining Pd-NZVI reactivity is its interaction with the stabilizing
381 surface modifiers. In this study, the relationship between surface modifiers types and doses and reactivity was
382 studied in batch reactors, and further studies of these interactions in packed sand columns and tanks under
383 NZVI injection conditions are needed to determine optimal surface modifier doses.

384 Rhamnolipids are very efficient for enhancing Pd-NZVI transport in the subsurface⁹, thus it was of interest to
385 us to measure the transport effectiveness of RL at the low loading of 13 mg TOC/g NZVI (Figure S10), where
386 its reactivity is not suppressed. Even at such low concentrations, RL is able to significantly enhance transport
387 compared to CMC-coated Pd-NZVI with an identical surface modifier loading or bare Pd-NZVI. Thus, for
388 overall efficient remediation, low concentrations of RL are desirable as they provide high reactivity and
389 efficient transport of Pd-NZVI. For CMC coated Pd-NZVI, the CMC dose may be chosen solely based on
390 effects on transport potential.

391 **SUPPORTING INFORMATION**

392 Details on GC, XPS, Cryo-TEM methods; XPS and FTIR data discussion; TCE degradation time profiles and
393 reaction end product distribution graphs, and RL- and CM- coated Pd-NZVI transport experiments.

394 **ACKNOWLEDGEMENTS**

395 This research was supported by the NSERC, Canada (Grant Nos. STPGP 365253-08; 203158-11 and
396 413978-12), Golder Associates Inc., and the FRQ-NT, Quebec, Canada (Grant No. 147187). We thank Ranjan
397 Roy and Andrew Golsztajn (McGill) for assisting with FTIR, TOC and ICP measurements; Kaustuv Basu,
398 Hojatollah Vali, S. Kelly Sears (McGill) for the Cryo-TEM analysis; and J. Lefebvre (Polytechnique
399 Montréal) for XPS analyses. S.B. and M.B. were supported by McGill Engineering Doctoral Awards.

400

401

402

403

404 **REFERENCES**

- 405 1. O'Carroll, D.; Sleep, B.; Krol, M.; Boparai, H.; Kocur, C., Nanoscale zero valent iron and bimetallic
406 particles for contaminated site remediation. *Adv. Water Resour.* **2013**, *51*, 104-122.
- 407 2. Reardon, E. J.; Fagan, R.; Vogan, J. L.; Przepiora, A., Anaerobic corrosion reaction kinetics of
408 nanosized iron. *Environ. Sci. Technol.* **2008**, *42*, (7), 2420-2425.
- 409 3. Sarathy, V.; Tratnyek, P. G.; Nurmi, J. T.; Baer, D. R.; Amonette, J. E.; Chun, C. L.; Penn, R. L.; Reardon,
410 E. J., Aging of iron nanoparticles in aqueous solution: effects on structure and reactivity. *J. Phys. Chem. C*
411 **2008**, *112*, (7), 2286-2293.
- 412 4. Phenrat, T.; Saleh, N.; Sirk, K.; Tilton, R. D.; Lowry, G. V., Aggregation and sedimentation of aqueous
413 nanoscale zerovalent iron dispersions. *Environ. Sci. Technol.* **2007**, *41*, (1), 284-290.
- 414 5. Dalla Vecchia, E.; Coisson, M.; Appino, C.; Vinai, F.; Sethi, R., Magnetic characterization and
415 interaction modeling of zerovalent iron nanoparticles for the remediation of contaminated aquifers. *J.*
416 *Nanosci. Nanotechnol.* **2009**, *9*, (5), 3210-3218.
- 417 6. Saleh, N.; Sirk, K.; Liu, Y.; Phenrat, T.; Dufour, B.; Matyjaszewski, K.; Tilton, R. D.; Lowry, G. V., Surface
418 modifications enhance nanoiron transport and NAPL targeting in saturated porous media. *Environ. Eng. Sci.*
419 **2007**, *24*, (1), 45-57.
- 420 7. He, F.; Zhao, D., Preparation and characterization of a new class of starch-stabilized bimetallic
421 nanoparticles for degradation of chlorinated hydrocarbons in water. *Environ. Sci. Technol.* **2005**, *39*, (9),
422 3314-3320.
- 423 8. He, F.; Zhao, D.; Liu, J.; Roberts, C. B., Stabilization of Fe-Pd nanoparticles with sodium
424 carboxymethyl cellulose for enhanced transport and dechlorination of trichloroethylene in soil and
425 groundwater. *Ind. Eng. Chem. Res* **2007**, *46*, (1), 29-34.
- 426 9. Basnet, M.; Ghoshal, S.; Tufenkji, N., Rhamnolipid biosurfactant and soy protein act as effective
427 stabilizers in the aggregation and transport of palladium-doped zerovalent iron nanoparticles in saturated
428 porous media. *Environ. Sci. Technol.* **2013**, *47*, (23), 13355-13364.
- 429 10. Cirtiu, C. M.; Raychoudhury, T.; Ghoshal, S.; Moores, A., Systematic comparison of the size, surface
430 characteristics and colloidal stability of zero valent iron nanoparticles pre-and post-grafted with common
431 polymers. *Colloids Surf. Physicochem. Eng. Aspects* **2011**, *390*, (1), 95-104.
- 432 11. Phenrat, T.; Saleh, N.; Sirk, K.; Kim, H.-J.; Tilton, R. D.; Lowry, G. V., Stabilization of aqueous nanoscale
433 zerovalent iron dispersions by anionic polyelectrolytes: adsorbed anionic polyelectrolyte layer properties and
434 their effect on aggregation and sedimentation. *J. Nanopart. Res.* **2008**, *10*, (5), 795-814.
- 435 12. Petosa, A. R.; Jaisi, D. P.; Quevedo, I. R.; Elimelech, M.; Tufenkji, N., Aggregation and deposition of
436 engineered nanomaterials in aquatic environments: role of physicochemical interactions. *Environ. Sci.*
437 *Technol.* **2010**, *44*, (17), 6532-6549.
- 438 13. Lien, H.-L.; Zhang, W.-x., Nanoscale iron particles for complete reduction of chlorinated ethenes.
439 *Colloids Surf. Physicochem. Eng. Aspects* **2001**, *191*, (1), 97-105.
- 440 14. Sakulchaicharoen, N.; O'Carroll, D. M.; Herrera, J. E., Enhanced stability and dechlorination activity of
441 pre-synthesis stabilized nanoscale FePd particles. *J. Contam. Hydrol.* **2010**, *118*, (3), 117-127.
- 442 15. Lien, H.-L.; Zhang, W.-X., Nanoscale Pd/Fe bimetallic particles: catalytic effects of palladium on
443 hydrodechlorination. *Appl. Catal., B* **2007**, *77*, (1), 110-116.
- 444 16. Lien, H.; Zhang, W., Effect of palladium on the reductive dechlorination of chlorinated ethylenes with
445 nanoscale Pd/Fe particles. *Water Supply* **2005**, *4*, (5-6), 297-303.
- 446 17. Zhu, B.-W.; Lim, T.-T., Catalytic reduction of chlorobenzenes with Pd/Fe nanoparticles: reactive sites,
447 catalyst stability, particle aging, and regeneration. *Environ. Sci. Technol.* **2007**, *41*, (21), 7523-7529.

- 448 18. Xie, Y.; Cwiertny, D. M., Chlorinated solvent transformation by palladized zerovalent iron:
449 Mechanistic insights from reductant loading studies and solvent kinetic isotope effects. *Environ. Sci. Technol.*
450 **2013**, *47*, (14), 7940-7948.
- 451 19. He, F.; Zhao, D., Hydrodechlorination of trichloroethene using stabilized Fe-Pd nanoparticles:
452 Reaction mechanism and effects of stabilizers, catalysts and reaction conditions. *Appl. Catal., B* **2008**, *84*, (3),
453 533-540.
- 454 20. Cho, Y.; Choi, S.-I., Degradation of PCE, TCE and 1, 1, 1-TCA by nanosized FePd bimetallic particles
455 under various experimental conditions. *Chemosphere* **2010**, *81*, (7), 940-945.
- 456 21. Zhou, H.; Han, J.; Baig, S. A.; Xu, X., Dechlorination of 2,4-dichlorophenoxyacetic acid by sodium
457 carboxymethyl cellulose-stabilized Pd/Fe nanoparticles. *J. Hazard. Mater.* **2011**, *198*, 7-12.
- 458 22. Phenrat, T.; Liu, Y.; Tilton, R. D.; Lowry, G. V., Adsorbed polyelectrolyte coatings decrease Fe0
459 nanoparticle reactivity with TCE in water: conceptual model and mechanisms. *Environ. Sci. Technol.* **2009**, *43*,
460 (5), 1507-1514.
- 461 23. Sun, Y.-P.; Li, X.-Q.; Zhang, W.-X.; Wang, H. P., A method for the preparation of stable dispersion of
462 zero-valent iron nanoparticles. *Colloids Surf. Physicochem. Eng. Aspects* **2007**, *308*, (1), 60-66.
- 463 24. Zhu, B.-W.; Lim, T.-T.; Feng, J., Influences of amphiphiles on dechlorination of a trichlorobenzene by
464 nanoscale Pd/Fe: adsorption, reaction kinetics, and interfacial interactions. *Environ. Sci. Technol.* **2008**, *42*,
465 (12), 4513-4519.
- 466 25. Basnet, M.; Di Tommaso, C.; Ghoshal, S.; Tufenkji, N., Reduced transport potential of a palladium-
467 doped zero valent iron nanoparticle in a water saturated loamy sand. *Water research* **2015**, *68*, 354-363.
- 468 26. Fatisson, J.; Ghoshal, S.; Tufenkji, N., Deposition of carboxymethylcellulose-coated zero-valent iron
469 nanoparticles onto silica: Roles of solution chemistry and organic molecules. *Langmuir* **2010**, *26*, (15), 12832-
470 12840.
- 471 27. Raychoudhury, T.; Naja, G.; Ghoshal, S., Assessment of transport of two polyelectrolyte-stabilized
472 zero-valent iron nanoparticles in porous media. *J. Contam. Hydrol.* **2010**, *118*, (3), 143-151.
- 473 28. Saleh, N.; Kim, H.-J.; Phenrat, T.; Matyjaszewski, K.; Tilton, R. D.; Lowry, G. V., Ionic strength and
474 composition affect the mobility of surface-modified Fe0 nanoparticles in water-saturated sand columns.
475 *Environ. Sci. Technol.* **2008**, *42*, (9), 3349-3355.
- 476 29. Goldman, S. M., Trichloroethylene and Parkinson's disease: dissolving the puzzle. **2010**.
- 477 30. Caldwell, J. C.; Keshava, N., Key issues in the modes of action and effects of trichloroethylene
478 metabolites for liver and kidney tumorigenesis. *Environ. Health Perspect.* **2006**, 1457-1463.
- 479 31. Kim, Y. H.; Carraway, E., Reductive dechlorination of TCE by zero valent bimetal. *Environ. Technol.*
480 **2003**, *24*, (1), 69-75.
- 481 32. Liu, Y.; Majetich, S. A.; Tilton, R. D.; Sholl, D. S.; Lowry, G. V., TCE dechlorination rates, pathways, and
482 efficiency of nanoscale iron particles with different properties. *Environ. Sci. Technol.* **2005**, *39*, (5), 1338-
483 1345.
- 484 33. He, F.; Zhao, D., Manipulating the size and dispersibility of zerovalent iron nanoparticles by use of
485 carboxymethyl cellulose stabilizers. *Environ. Sci. Technol.* **2007**, *41*, (17), 6216-6221.
- 486 34. Kim, H.-J.; Phenrat, T.; Tilton, R. D.; Lowry, G. V., Fe0 nanoparticles remain mobile in porous media
487 after aging due to slow desorption of polymeric surface modifiers. *Environ. Sci. Technol.* **2009**, *43*, (10), 3824-
488 3830.
- 489 35. Phenrat, T.; Kim, H.-J.; Fagerlund, F.; Illangasekare, T.; Tilton, R. D.; Lowry, G. V., Particle size
490 distribution, concentration, and magnetic attraction affect transport of polymer-modified Fe0 nanoparticles
491 in sand columns. *Environ. Sci. Technol.* **2009**, *43*, (13), 5079-5085.
- 492 36. Jiemvarangkul, P.; Zhang, W.-x.; Lien, H.-L., Enhanced transport of polyelectrolyte stabilized
493 nanoscale zero-valent iron (nZVI) in porous media. *Chem. Eng. J.* **2011**, *170*, (2), 482-491.

- 494 37. Yan, W.; Herzing, A. A.; Li, X.-q.; Kiely, C. J.; Zhang, W.-x., Structural evolution of Pd-doped nanoscale
495 zero-valent iron (nZVI) in aqueous media and implications for particle aging and reactivity. *Environ. Sci.*
496 *Technol.* **2010**, *44*, (11), 4288-4294.
- 497 38. Ling, L.; Zhang, W.-X., Structures of Pd–Fe (0) bimetallic nanoparticles near 0.1 nm resolution. *RSC*
498 *Adv.* **2014**, *4*, (64), 33861-33865.
- 499 39. Burris, D. R.; Delcomyn, C. A.; Smith, M. H.; Roberts, A. L., Reductive dechlorination of
500 tetrachloroethylene and trichloroethylene catalyzed by vitamin B12 in homogeneous and heterogeneous
501 systems. *Environ. Sci. Technol.* **1996**, *30*, (10), 3047-3052.
- 502 40. Wang, C.-B.; Zhang, W.-X., Synthesizing nanoscale iron particles for rapid and complete
503 dechlorination of TCE and PCBs. *Environ. Sci. Technol.* **1997**, *31*, (7), 2154-2156.
- 504 41. Lowry, G. V.; Gregory, K. B.; Apte, S. C.; Lead, J. R., Transformations of nanomaterials in the
505 environment. *Environ. Sci. Technol.* **2012**, *46*, (13), 6893-6899.
- 506 42. Scamehorn, J.; Schechter, R.; Wade, W., Adsorption of surfactants on mineral oxide surfaces from
507 aqueous solutions: I: Isomerically pure anionic surfactants. *J. Colloid Interface Sci.* **1982**, *85*, (2), 463-478.
- 508 43. Ochoa-Loza, F. J.; Artiola, J. F.; Maier, R. M., Stability constants for the complexation of various
509 metals with a rhamnolipid biosurfactant. *J. Environ. Qual.* **2001**, *30*, (2), 479-485.

510

511

512

513

514

515

516

517

518

519

520 **List of Figures:**

521 **Figure 1:** (a1-a2) HR-TEM of uncoated Pd-NZVI (b1)Cryo TEM of uncoated Pd-NZVI (b2) Cryo TEM of RL-
522 coated-Pd-NZVI (b3) Cryo TEM of CMC-coated-Pd-NZVI

523

524 **Figure 2:** Pseudo first order TCE degradation rate constants for Pd-NZVI at different surface modifier
525 loadings in the reaction systems. Error bars represent standard deviation of measurements from triplicate
526 reactors

527

528 **Figure 3:** Effect of surface modifier type and dose on palladium deposition. Error bars on histograms
529 represent standard deviation of triplicates. Texts in bold alongside the histogram represent the TCE
530 degradation rate constants obtained with Pd-NZVI particles at a given total surface modifier loading. The
531 remainder of undeposited palladium was measured in the supernatant and >99% mass balance was obtained.

532

533

534 **Figure 4:** (a) Adsorbed surface modifier amounts with varying total surface modifier loadings. Solid lines are
535 drawn to guide the eye. (b) RL adsorption to NZVI fitted with Langmuir isotherm, where q_e is the equilibrium
536 adsorption capacity of NZVI, C_e is the equilibrium aqueous phase concentration of RL, q_m is the maximum
537 adsorption capacity of NZVI and K_a is the adsorption equilibrium constant (c) CMC adsorption to NZVI fitted
538 with Freundlich isotherm, where K_F and n are empirical constants. Error bars represent standard deviation of
539 triplicates.

540

541 **Figure 5:** Schematic illustrating Pd-NZVI interactions in (a) absence of any surface modifier, (b) at low and
542 high CMC loadings, (c) at low RL loading and, (d) at high RL loading

543

544 **Figure 6:** (a) TCE degradation by RL coated Pd-NZVI particles in the presence and absence of excess RL in
545 solution. Error bars represent standard deviation of triplicates. Lines through data points are drawn to guide
546 the eye. (b) Schematic of Pd, RL and Pd-NZVI interactions in the presence of RL in solution (c) Schematic of
547 Pd, RL and Pd-NZVI interactions and TCE reactions in the absence of RL in solution.

548

549

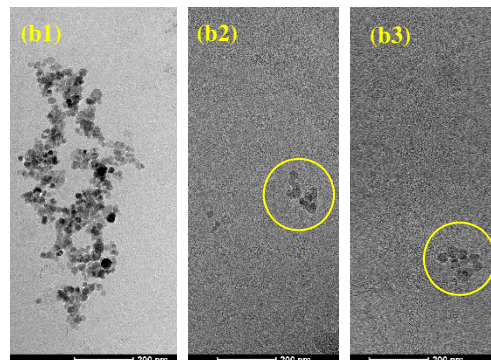
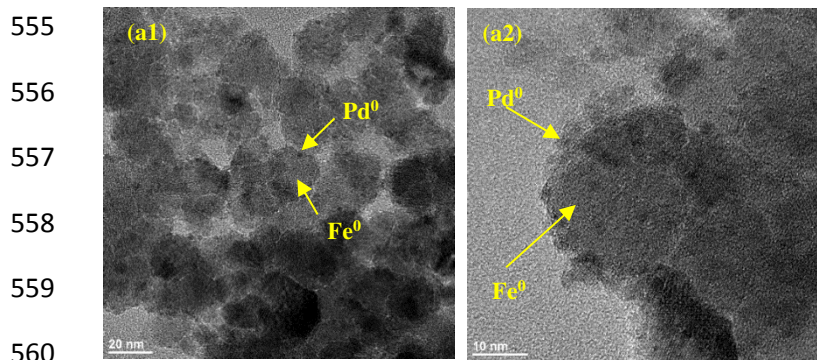
550

551

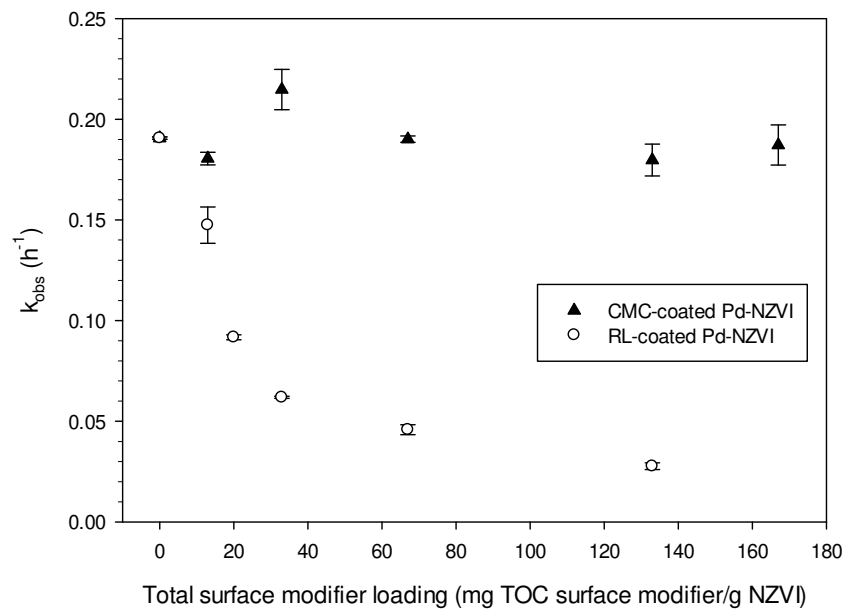
552

553

554 **Figure 1:**



580 **Figure 2:**



581

582

583

584

585

586

587

588

589

590

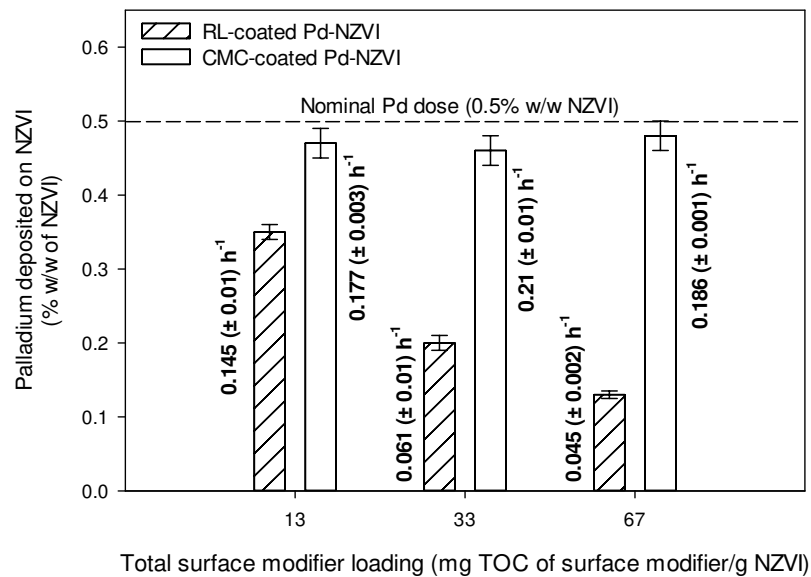
591

592

593

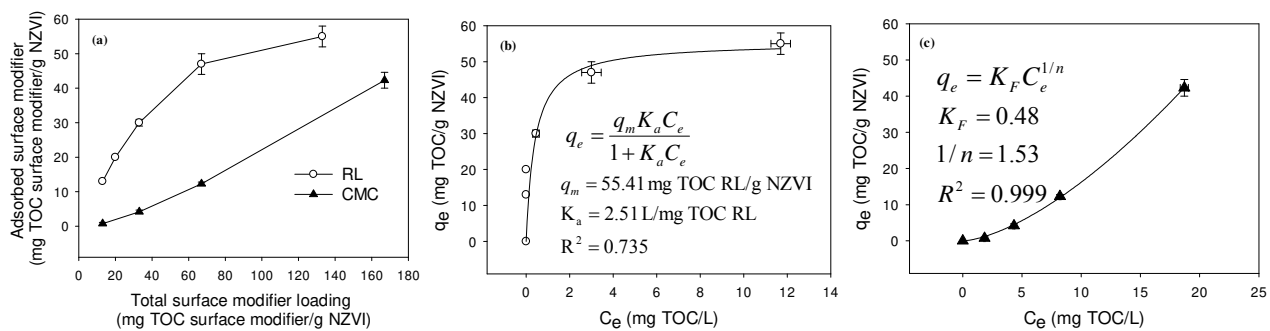
594

595 **Figure 3:**



596
597
598
599
600
601
602
603
604
605
606
607
608
609
610

611 **Figure 4:**



612

613

614

615

616

617

618

619

620

621

622

623

624

625

626

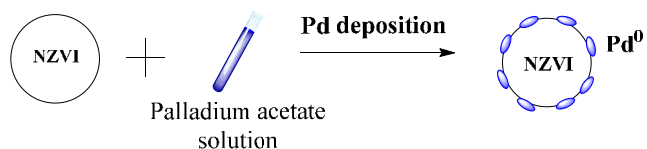
627

628

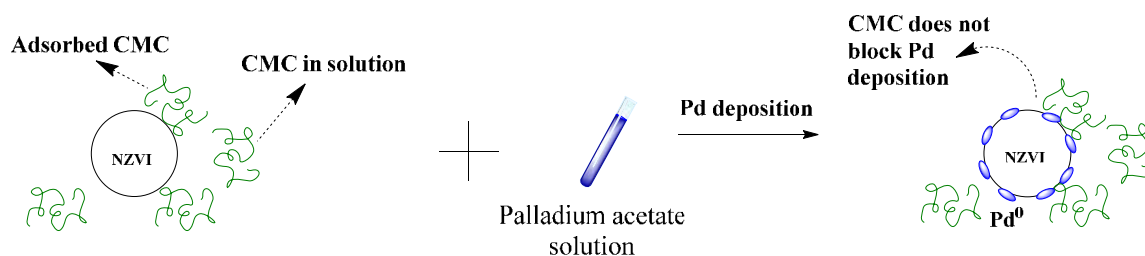
629 **Figure 5:**

630

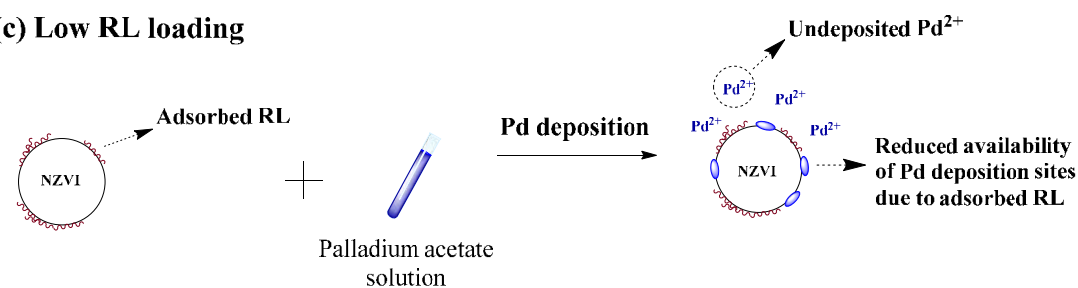
(a) Pd-NZVI



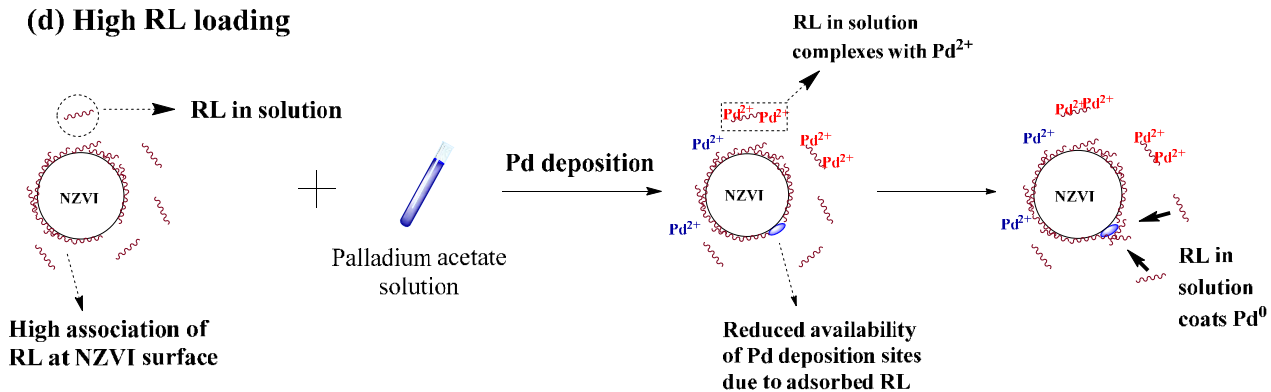
(b) Low and high CMC loading



(c) Low RL loading



(d) High RL loading

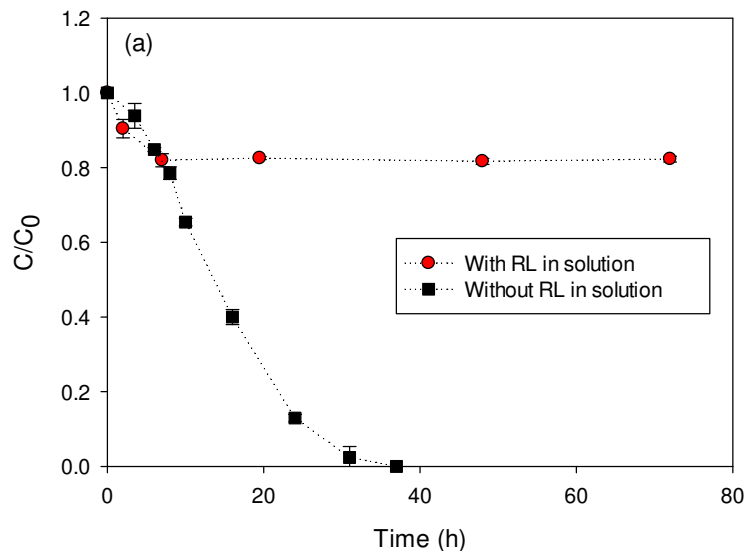


631

632

633

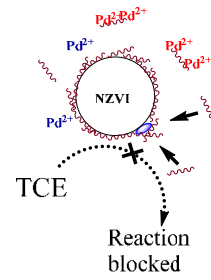
634 **Figure 6:**



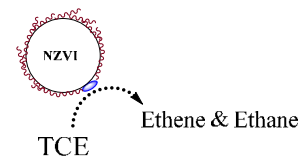
635

636

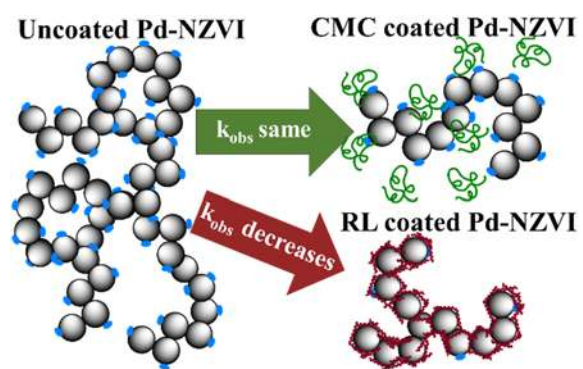
(b) With RL in solution



(c) Without RL in solution



637 **TOC**



638

Supporting Information

Effects of rhamnolipid and carboxymethylcellulose coatings on reactivity of palladium-doped nanoscale zerovalent iron particles

Sourjya Bhattacharjee¹, Mohan Basnet², Nathalie Tufenkji², Subhasis Ghoshal^{1*}

¹Department of Civil Engineering, McGill University, Montreal, QC H3A 0C3, Canada

²Department of Chemical Engineering, McGill University, Montreal, QC H3A 0C5, Canada

Number of pages: 11

Number of tables: 2

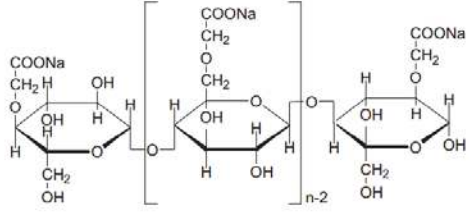
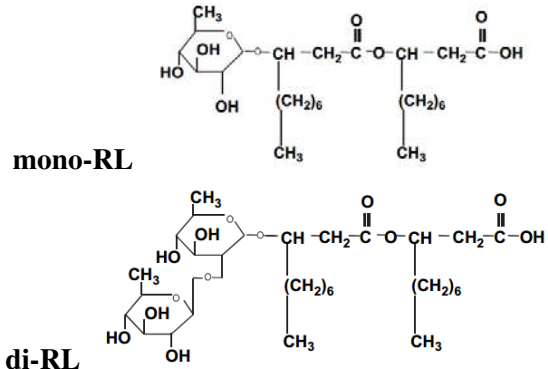
Number of figures: 10

Journal: Environmental Science and Technology

*Corresponding author phone: 514-398-6867; fax: 514-398-7361; email: subhasis.ghoshal@mcgill.ca

26
27
28

Table S1: Details of surface modifiers used in the study. Structure of CMC adapted from Cirtiu et al.¹ and structure of RL adapted from Mulligan².

Surface Modifier	Composition	Molecular weight	Structure
Carboxymethyl-cellulose (CMC)	polyelectrolyte with sodium as a counter ion to the carboxyl group	700 kDa	
Rhamnolipid (RL)	aqueous solution containing mixture of mono- and dirhamnolipid	mono-RL: 504 Da di-RL: 650 Da	

29

30 METHODS

31 GC-FID:

32 TCE was quantified by direct injection of 300 μ L of reactor headspace into a Varian CP 3800 GC with
33 flame ionization detector fitted with a GS-Q plot column (0.53 mm \times 30 m, Agilent). 1000 ppm
34 calibration gas standard of ethane, ethene and acetylene was obtained in nitrogen from Scotty Specialty
35 Gases. Samples were injected in split-less mode at 250 $^{\circ}$ C injector temperature and oven temperature held
36 at 50 $^{\circ}$ C for 2 min, followed by a ramp of 40 $^{\circ}$ C/min to 200 $^{\circ}$ C and then held at that temperature for 5 min.

37 X-ray Photoelectron Spectroscopy (XPS):

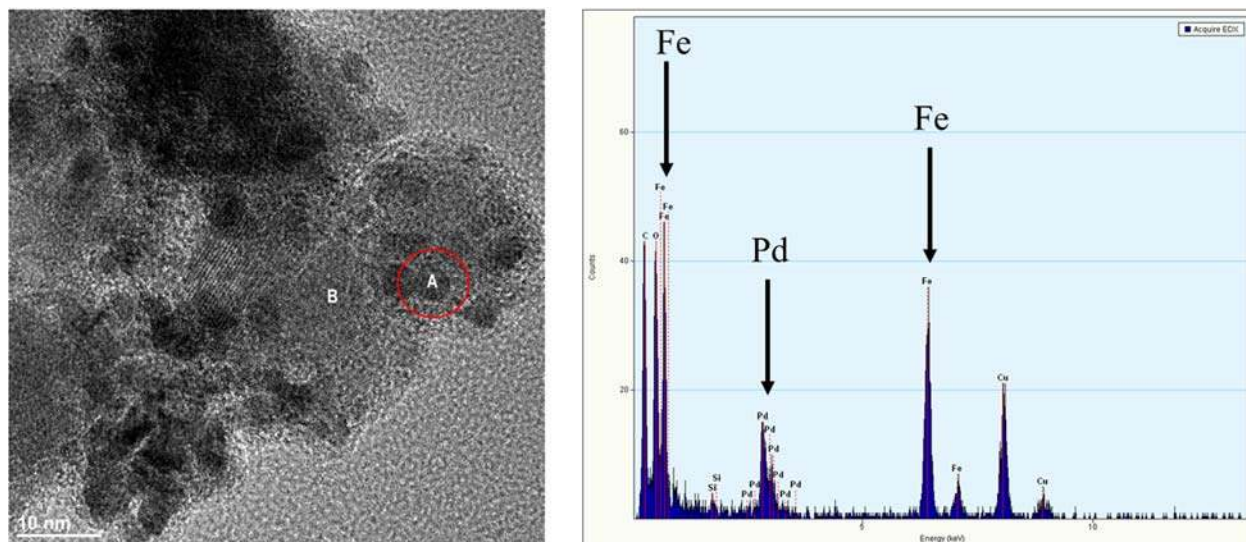
38 XPS was performed for bare NZVI using a VG Escalab 3MKII instrument to characterize the surface
39 oxide layer. Dried NZVI was irradiated using an Al K α source at a power of 300 W (15 kV, 20 mA). The
40 binding energies of the photoelectrons were calibrated by the aliphatic adventitious hydrocarbon C 1s
41 peak at 285.0 eV with survey scan of energy step of 1.0 eV, pass energy of 100 eV and high resolution
42 scans with energy step of 0.05 eV, pass energy of 20 eV.

43 Cryogenic-Transmission Electron Microscopy:

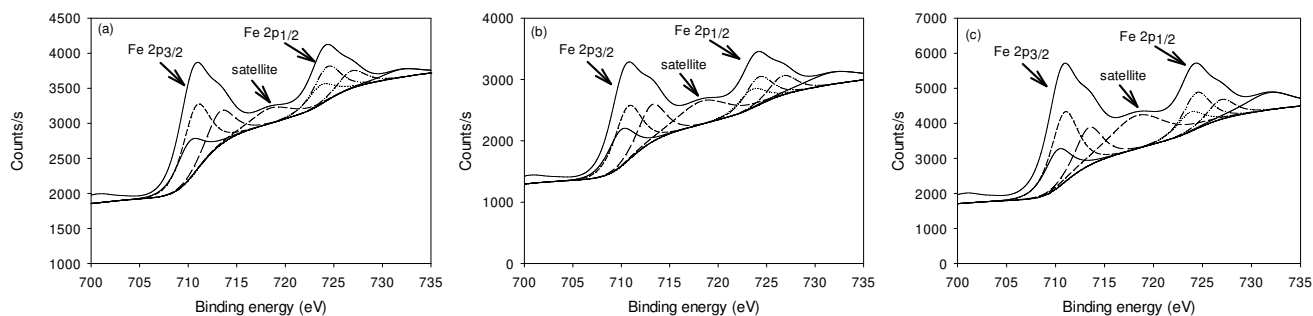
44 Cryogenic-Transmission electron microscopy (Cryo-TEM) was performed on uncoated Pd-NZVI and RL
45 and CMC-coated Pd-NZVI to observe the aggregate structure of nanoparticles in solution. 3 μ l of sample

46 (Pd-NZVI suspension -1 g/L) was added to C-Flat 2/2 EM grids (Protochips). Excess fluid was blotted
 47 and the sample was flash frozen hydrated by plunging into a bath of liquid ethane using FEI Vitrobot Grid
 48 Plunging System (FEI electron optics). The grids were then stored in liquid nitrogen until observation.
 49 Images were acquired using FEI Titan Krios 300kv CryoS/TEM microscope (FEI,Inc) equipped with
 50 Falcon 2 Direct Detection Device (DDD)(FEI) at a magnification of 29000 \times corresponding to a 2.84 A
 51 pixel size of (defocus level ranging from -2.0 to $-3.0\mu\text{m}$) under low dose conditions.

52 RESULTS AND DISCUSSION



53
 54 **Figure S1:** TEM-EDS performed on spot A of uncoated Pd-NZVI (spectra shown in right hand image)
 55



56
 57 **Figure S2:** Narrow scans of Fe2p XPS spectra for (a) Uncoated NZVI (b) RL-coated NZVI (c) CMC-
 58 coated NZVI
 59

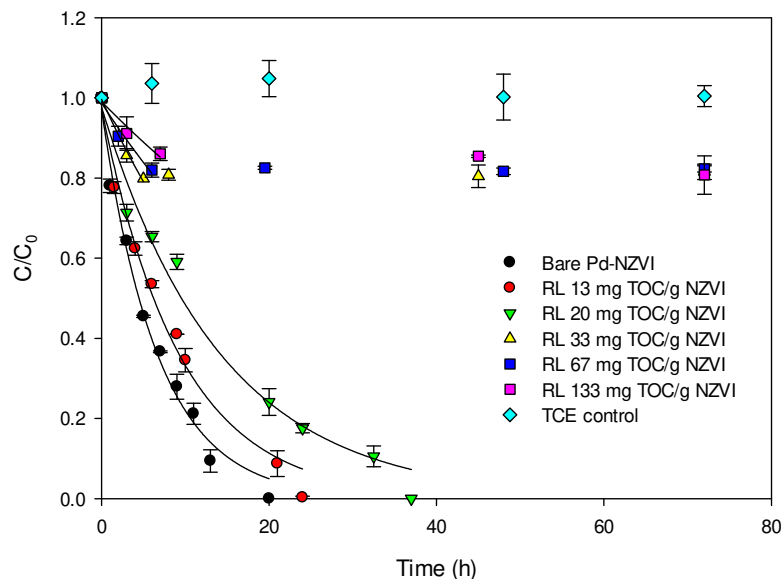
60 X-ray Photoelectron Spectroscopy (XPS)

62 XPS analyses were conducted for uncoated NZVI, RL-coated NZVI and CMC-coated NZVI as shown in
 63 Figure S2 (a), (b) and (c) respectively. The spectra of RL-coated and CMC-coated NZVI were similar to
 64 the uncoated NZVI indicating that coating with surface modifiers did not alter the chemical state of the
 65 NZVI.

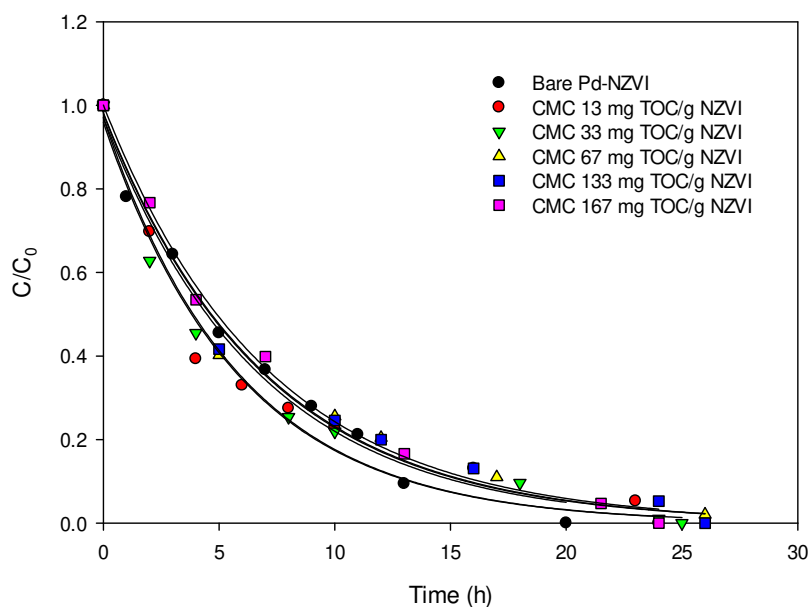
66 The low resolution spectra for uncoated NZVI indicated the presence of Fe and O on the surface. Based
67 on high resolution scans for the Fe 2p_{3/2} spectra (Figure S1 a), deconvoluted peaks were obtained for
68 Fe(II) and Fe(III) oxidation states between 710.0 eV and 713.3 eV. Peaks with binding energies of 710.1,
69 710.8 and 713.3 suggest the presence of FeO, Fe₂O₃ and FeOOH.^{3,4} No signal was detected for Fe(0) and
70 can be attributed to the fact that X-ray probing depth was less than 5 nm. High resolution scans for
71 oxygen (data not shown) reveal peaks at binding energies of 530.3 and 531.9 which also suggest the
72 formation of oxide and hydroxide species of Fe.³

73 **Electrophoretic mobility and Zeta potential:**

74 Electrophoretic mobility (EPM) and zeta potential (ZP) of the NZVI particles used in this study have been
75 previously reported⁵ and for 3 mM NaCl ionic strength and a pH of 7.7±0.2, an EPM of -1.9 ± 0.3
76 µm.cm/V.s was obtained for which the equivalent ZP was calculated as -26.4±3.4 mV.



77
78 **Figure S3:** TCE degradation profiles as a function of time for RL-coated Pd-NZVI particles at different
79 total RL loadings. Error bars represent standard deviation of triplicates. Lines through the data points
80 are pseudo first order fits ($r^2 > 0.98$). For RL loadings 33 to 133 mg TOC/g NZVI, only first three data
81 points were fitted to the model (where $r^2 > 0.98$) due to no further degradation beyond the initial time
82 points.



83

84 **Figure S4:** TCE degradation profiles as a function of time for CMC-coated Pd-NZVI particles at different
 85 polyelectrolyte loadings. Error bars represent standard deviation of triplicates. Lines through the data
 86 points are pseudo first order fits ($r^2 > 0.98$).

87 **Calculation of k_{obs}**

88 Values of k_{obs} were corrected as described in other studies^{6,7} to account for the effects of
 89 partitioning of the reactant between the aqueous and gas phases, using the following equation:

90
$$k_{obs} = k'_{obs} \left(1 + \frac{V_g}{V_w} K_H \right) \quad (S1)$$

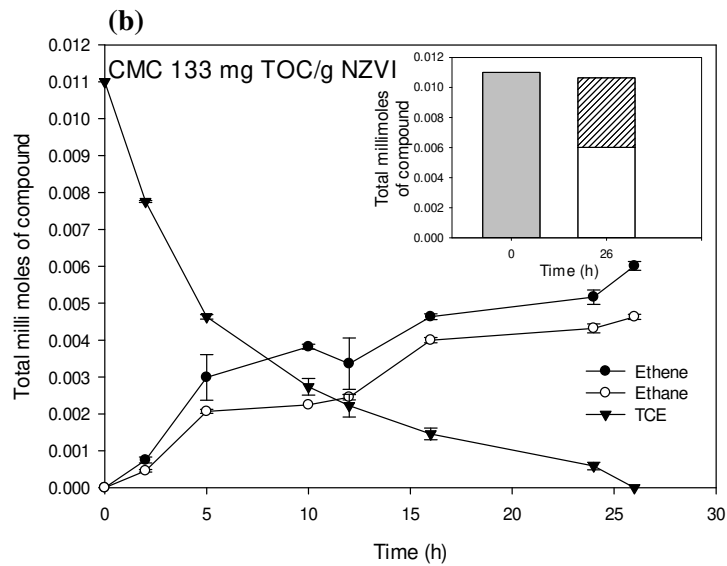
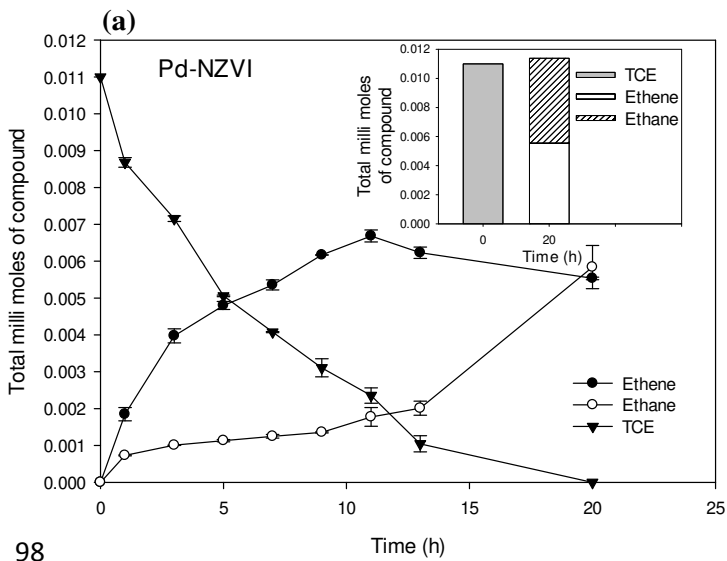
91 where, k'_{obs} is the pseudo-first-order rate constants determined by best fit of measured aqueous
 92 concentrations as a function of time to a pseudo first-order rate law, while, V_w , V_g and K_H are the
 93 aqueous volume, headspace volume and the dimensionless Henry's coefficient.

94

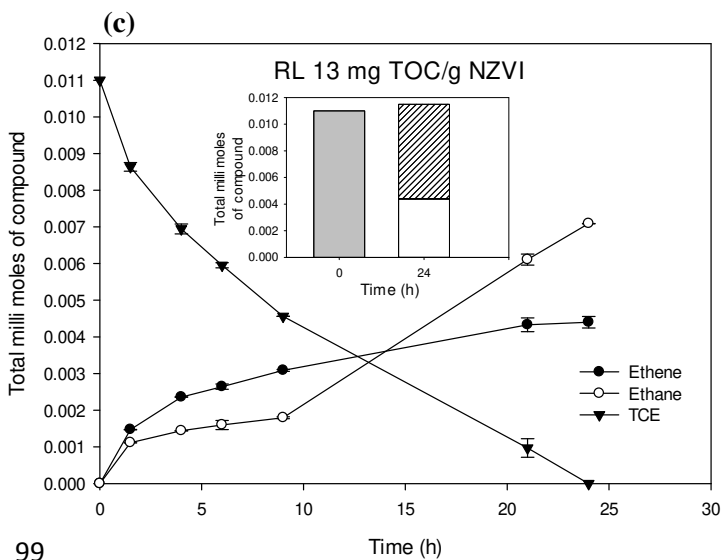
95 **Table S2:** DLS hydrodynamic diameters for Pd-NZVI particles at different times in DI water

Time (h)	Hydrodynamic diameters (nm)				
	Uncoated Pd-NZVI	RL-Pd-NZVI		CMC-Pd-NZVI	
		13 mg TOC/g NZVI	67 mg TOC/g NZVI	13 mg TOC/g NZVI	67 mg TOC/g NZVI
5	1000±107	215±14	305±15	289±10	329±86
15	1566±303	323±76	300±56	375±80	340±72
40	1600±208	293±109	297±50	295±25	338±54

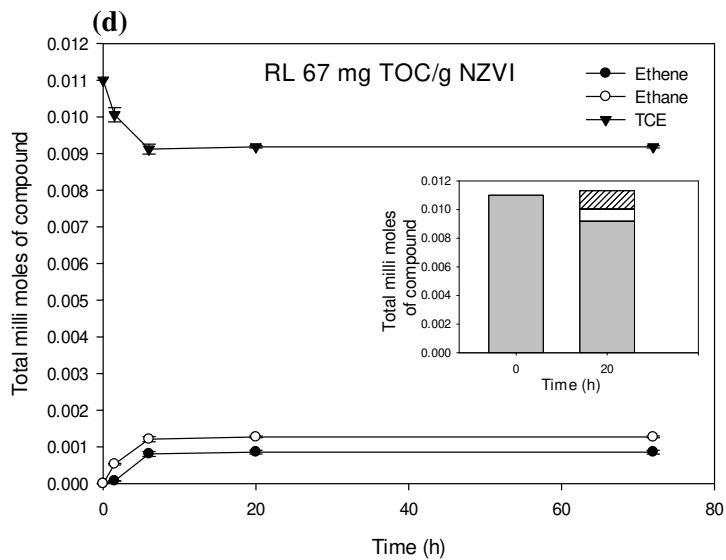
96



98



99



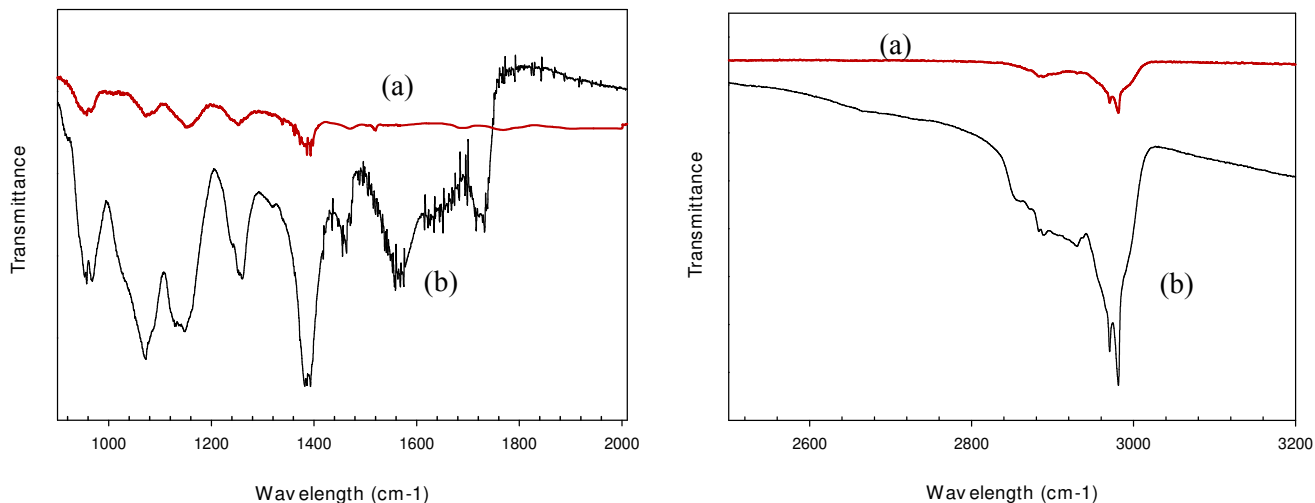
100 **Figure S5:** TCE degradation and end product evolution time profile for (a) Pd-NZVI (b) CMC-coated Pd-
 101 NZVI at total CMC loading of 133 mg TOC/g NZVI (c) Rhamnolipid-coated Pd-NZVI at total RL loading of
 102 13 mg TOC/g NZVI (d) Rhamnolipid-coated Pd-NZVI at total RL loading of 67 mg TOC/g NZVI). Insets
 103 represent total mass balances at end of reaction. Ethene and ethane were the reaction end-products. For all
 104 reactor systems studied, mass balance achieved was >90%.

105

106

107

108



109

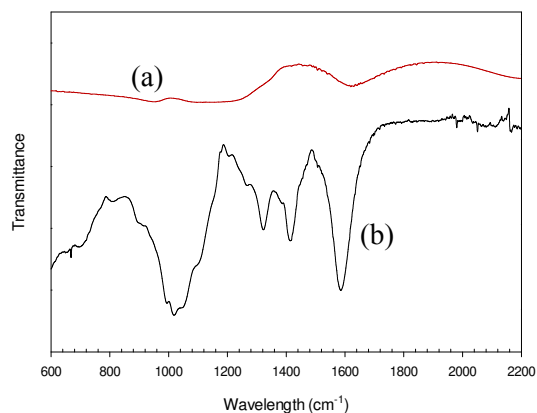
110

Figure S6: FTIR spectra of (a) RL-coated NZVI (b) RL

111 Figure S6 shows the FTIR spectrum of (a) RL coated NZVI and (b) RL.

112 **RL spectra:** The major peaks in the 3000-2800 cm^{-1} region are the $\nu_{\text{asym}}(\text{CH}_2)$ and $\nu_{\text{sym}}(\text{CH}_2)$ modes at
 113 2960 and 2880 cm^{-1} , respectively. The low frequency region is dominated by the carboxylic acid
 114 $\nu_{\text{sym}}(\text{C}=\text{O})$ stretch at 1730 cm^{-1} and the $\nu_{\text{asym}}(\text{COO}^-)$ carboxylate mode at 1560 cm^{-1} . The region below
 115 1500 cm^{-1} corresponds to the fingerprint region for rhamnolipid which includes vibrational modes of the
 116 rhamnose head group.^{8,9}

117 **RL coated NZVI spectra:** The asymmetric and symmetric CH_2 stretch did not show any change in the
 118 peak positions. However the $\nu_{\text{asym}}(\text{COO}^-)$ carboxylate mode shifted to 1520 cm^{-1} while the peak at
 119 $\nu_{\text{sym}}(\text{C}=\text{O})$ appeared to be split into a doublet. However the peak intensity isn't strong enough to conclude
 120 the splitting of the peak. However, overall it appears, that the interaction of rhamnolipid at the NZVI
 121 surface is through the carboxylate group.



122

123

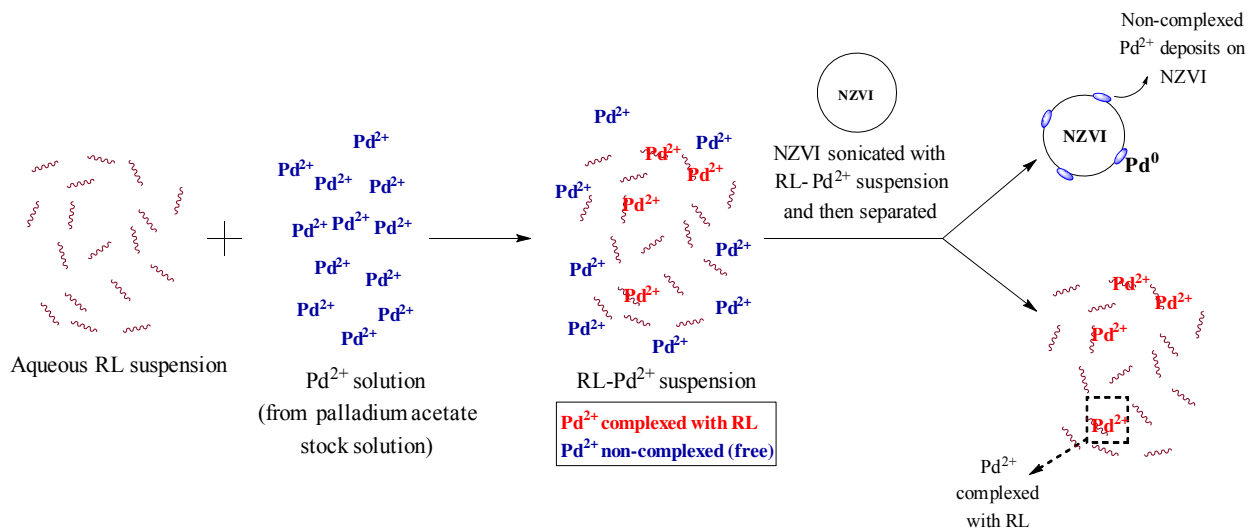
Figure S7: FTIR spectra of (a) CMC coated NZVI (b) CMC

124 Figure S7 shows the FTIR spectrum of (a) CMC coated NZVI and (b) CMC.

125 **CMC spectra:** The peaks observed at 1590 cm^{-1} and 1410 cm^{-1} are the $\nu_{\text{asym}}(\text{COO}^-)$ and $\nu_{\text{sym}}(\text{COO}^-)$ as
126 well as the remaining peaks observed are in agreement with Cirtiu et. al¹.

127 **CMC coated NZVI spectra:** It was observed that the $\nu_{\text{asym}}(\text{COO}^-)$ carboxylate stretch shifted to 1610 cm^{-1}
128 ¹ indicating CMC interacted with NZVI through the carboxylate group.

129



130
131 *Figure S8: Schematic demonstrating the experimental design to quantify complexation by RL.*

132 **RL- Pd²⁺ Complexation:**

133 In TCE degradation experiments, the system with total RL loading of 67 mg TOC/g NZVI, has

- 134 (a) RL in solution = 3 mg TOC/L, and
135 (b) RL adsorbed to NZVI surface = 40 mg TOC/g NZVI (Figure 4 in Manuscript).

136 **PART I:** First we quantified how much Pd²⁺ was complexed by 3 mg TOC/L RL.

137 We designed an experiment using uncoated NZVI as shown in Figure S8.

- 138 (1) First, an aqueous suspension of 3 mg TOC/L RL was mixed with 0.75 mg/L Pd²⁺ (0.5% w/w of
139 150 mg/L NZVI) for 10 minutes.
140 (2) Thereafter, the RL-Pd²⁺ suspension was sonicated with 150 mg/L NZVI for 15 minutes.
141 Within a timeframe of 15 minutes, no RL sorbs to NZVI. Thus, in this step, the amount of Pd
142 that deposits on NZVI can be attributed to Pd⁰ and it is derived from the free Pd²⁺ in the RL-Pd²⁺
143 suspension prior to contact with NZVI.
144 (3) The supernatant was then decanted after centrifugation and retention of the NZVI with a super-
145 magnet.
146 (4) The separated NZVI (with Pd⁰ deposits on its surface) was then acid digested and analyzed in
147 ICP-OES for quantification of Pd. This gives us the amount of non-complexed/free Pd²⁺ in the
148 RL- Pd²⁺ suspension prior to contact with NZVI.
149 (5) The supernatant was then acid digested and analyzed in ICP-OES to quantify the remainder of the
150 Pd²⁺ (which did not deposit on NZVI in step 2) and was attributed to the amount of Pd²⁺
151 complexed with RL.

152 The mixing times between RL and Pd²⁺ was fixed based on their interaction time during synthesis
153 of RL-coated Pd-NZVI in the TCE degradation experiments. No sorption of the of RL onto NZVI
154 surface occurred during the 15 minute sonication time between NZVI and RL- Pd²⁺ suspension as
155 confirmed through TOC analysis.

156 The experiment showed that, for a 0.03 mg nominal Pd dose,

- 157 • 0.009(±0.001) mg Pd was complexed with 3 mg/L RL,
- 158 • while 0.021(±0.001) mg Pd deposited on uncoated NZVI (which we attributed to non-
- 159 complexed Pd²⁺).

160 **PART II:** In the next step we compared the amount of Pd deposited on

- 161 (i) uncoated NZVI (measured in Part I) and
- 162 (ii) the Pd deposited on NZVI coated with RL 40 mg TOC/g NZVI

163 Pd deposited on uncoated NZVI was 0.0021 mg (measured in part I).

164 We measured Pd deposited on the RL-coated NZVI to be 0.0078 mg.

165 Therefore the lower deposition on the RL-coated NZVI, is attributed to the lesser number of Pd
166 deposition sites due to surface sorbed RL.

167 The amount of Pd²⁺ that did not deposit on RL-coated NZVI due to decrease in deposition sites, is
168 0.0132 mg Pd (0.021mg-0.0078mg)

169

170 Overall by combining PART I and PART II, we know:

171 Pd²⁺ complexed with 3 mg TOC/L RL = 0.009 mg

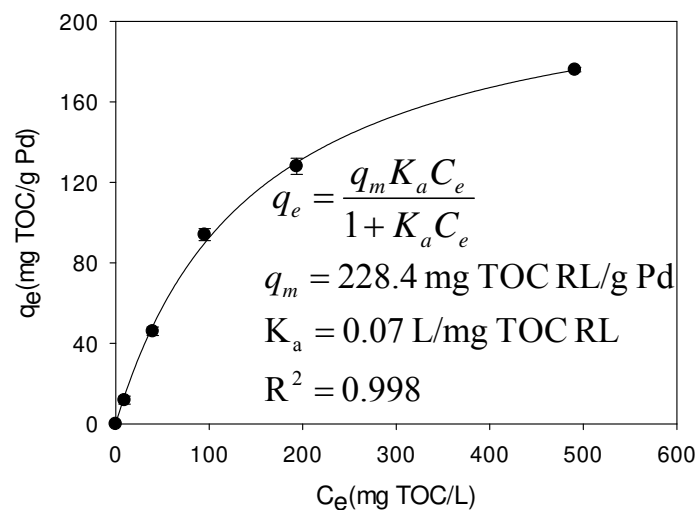
172 Pd²⁺ deposited on NZVI coated with RL 40 mg TOC/g NZVI = 0.0078 mg

173 Pd²⁺ undeposited = 0.0132 mg Pd

174

175

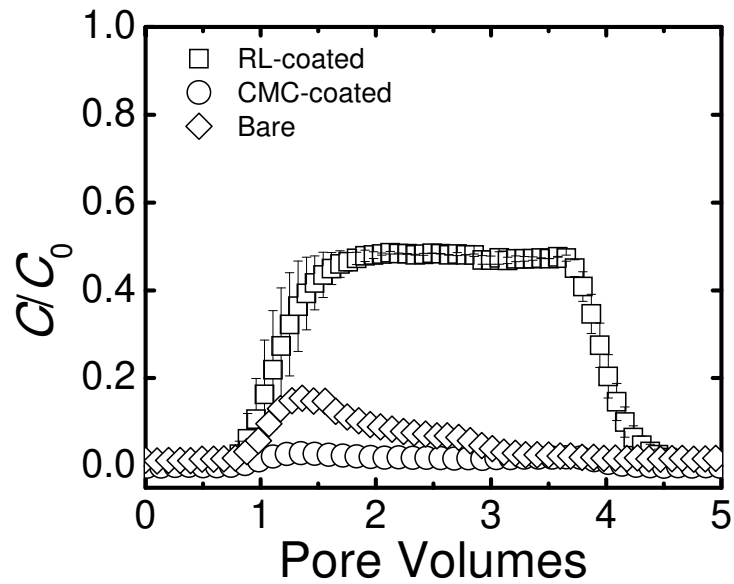
176



177

178 **Figure S9:** Sorption of RL to Pd⁰ nanoparticles fitted with Langmuir isotherm, where q_e is the
 179 equilibrium adsorption capacity of Pd⁰, C_e is the equilibrium aqueous phase concentration of RL, q_m is
 180 the maximum adsorption capacity of Pd⁰ and K_a is the adsorption equilibrium constant.

181 Pd⁰ nanoparticle synthesis: Palladium nanoparticles were synthesized using methods described
 182 previously^{10, 11} with certain modifications. 50 mg of Pd-acetate was added to 50 mL de-ionized water and
 183 sonicated for 5 minutes. The suspension turned yellowish-orange due to dissolution of Pd-acetate in
 184 water. 40 mL of the supernatant containing aqueous solution of Pd-acetate was then removed and mixed
 185 in a round-bottom flask using a magnetic stirrer for 15 minutes under N₂ flow. 10 mL of 1.5 g/L of
 186 sodium borohydride was then added drop-wise to the Pd-acetate solution which instantly turned black
 187 indicating the formation of Pd⁰ nanoparticles. The suspension was mixed for 1 hour. The concentration of
 188 Pd⁰ nanoparticles was determined using ICP-OES analysis and the nanoparticles were sized using
 189 Nanoparticle tracking analysis (NanoSight LM14). The mean size of nanoparticles obtained were 150±30
 190 nm. Stabilizing polymers to obtain highly monodisperse Pd⁰ or solvents such as ethanol to improve
 191 aqueous solubility of palladium acetate were not implemented in this synthesis because they interfere
 192 during the TOC analysis for determining the sorption isotherm as in Figure S9. The sorption isotherm was
 193 determined using similar procedures as described in the manuscript.



194

195 **Figure S10:** Measured breakthrough curves for rhamnolipid- and CMC- coated Pd-NZVI at 10 mM
 196 NaHCO₃ and pH 7.7. The surface modifier loading used was 13 mg TOC/g NZVI for both rhamnolipid
 197 and CMC. The transport experiments were conducted in a clean quartz sand column (mean grain size 651
 198 μm and porosity 0.38) with an approach velocity of 7.5×10^{-5} m/s. (According to methods described in
 199 Basnet et al.¹²)

200

- 202 1. Cirtiu, C. M.; Raychoudhury, T.; Ghoshal, S.; Moores, A., Systematic comparison of the size,
203 surface characteristics and colloidal stability of zero valent iron nanoparticles pre-and post-grafted with
204 common polymers. *Colloids Surf. Physicochem. Eng. Aspects* **2011**, *390*, (1), 95-104.
- 205 2. Mulligan, C. N., Environmental applications for biosurfactants. *Environmental pollution* **2005**,
206 *133*, (2), 183-198.
- 207 3. McIntyre, N.; Zetaruk, D., X-ray photoelectron spectroscopic studies of iron oxides. *Analytical*
208 *Chemistry* **1977**, *49*, (11), 1521-1529.
- 209 4. Jeong, H. Y.; Han, Y.-S.; Park, S. W.; Hayes, K. F., Aerobic oxidation of mackinawite (FeS) and its
210 environmental implication for arsenic mobilization. *Geochimica et Cosmochimica Acta* **2010**, *74*, (11),
211 3182-3198.
- 212 5. Basnet, M.; Di Tommaso, C.; Ghoshal, S.; Tufenkji, N., Reduced transport potential of a
213 palladium-doped zero valent iron nanoparticle in a water saturated loamy sand. *Water research* **2015**,
214 *68*, 354-363.
- 215 6. Burris, D. R.; Delcomyn, C. A.; Smith, M. H.; Roberts, A. L., Reductive dechlorination of
216 tetrachloroethylene and trichloroethylene catalyzed by vitamin B12 in homogeneous and
217 heterogeneous systems. *Environ. Sci. Technol.* **1996**, *30*, (10), 3047-3052.
- 218 7. Rajajayavel, S. R. C.; Ghoshal, S., Enhanced reductive dechlorination of trichloroethylene by
219 sulfidated nanoscale zerovalent iron. *Water research* **2015**, *78*, 144-153.
- 220 8. Lebron-Paler, A., *Solution and Interfacial Characterization of Rhamnolipid Biosurfactant from*
221 *Pseudomonas aeruginosa ATCC 9027*. ProQuest: 2008.
- 222 9. Leitermann, F.; Syldatk, C.; Hausmann, R., Fast quantitative determination of microbial
223 rhamnolipids from cultivation broths by ATR-FTIR Spectroscopy. *Journal of biological engineering* **2008**,
224 *2*, (1), 1-8.
- 225 10. NaiduáKona, C., A simple method for the preparation of ultra-small palladium nanoparticles and
226 their utilization for the hydrogenation of terminal alkyne groups to alkanes. *Nanoscale* **2015**, *7*, (3), 872-
227 876.
- 228 11. Ugalde-Saldivar, V., Aerobic synthesis of palladium nanoparticles. *Rev. Adv. Mater. Sci* **2011**, *27*,
229 31-42.
- 230 12. Basnet, M.; Ghoshal, S.; Tufenkji, N., Rhamnolipid biosurfactant and soy protein act as effective
231 stabilizers in the aggregation and transport of palladium-doped zerovalent iron nanoparticles in
232 saturated porous media. *Environ. Sci. Technol.* **2013**, *47*, (23), 13355-13364.